

# Lawrence Berkeley National Laboratory

## Recent Work

### Title

The Dynamics of Electronic to Vibrational, Rotational and Translational Energy Transfer in Collision of Ba(<sup>1</sup>P<sub>1</sub>) with Diatomic Molecules

### Permalink

<https://escholarship.org/uc/item/3s28d4xw>

### Journal

Journal of Chemical Physics, 97(6)

### Authors

Suits, Arthur G.  
Pujo, P. de  
Sublemontier, O.  
[et al.](#)

### Publication Date

1992-05-01



# Lawrence Berkeley Laboratory

UNIVERSITY OF CALIFORNIA

## CHEMICAL SCIENCES DIVISION

Submitted to Journal of Chemical Physics

### The Dynamics of Electronic to Vibrational, Rotational and Translational Energy Transfer in Collision of Ba( $^1P_1$ ) with Diatomic Molecules

A.G. Suits, P. de Pujo, O. Sublemontier, J.-P. Visticot, J. Berlande, J. Cuvellier, T. Gustavsson, J.-M. Mestdagh, P. Meynadier, and Y.T. Lee

May 1992



REFERENCE COPY |  
Does Not |  
Circulate |  
BLDG. 50 Library.  
LBL-32441  
Copy 1

#### DISCLAIMER

This document was prepared as an account of work sponsored by the United States Government. Neither the United States Government nor any agency thereof, nor The Regents of the University of California, nor any of their employees, makes any warranty, express or implied, or assumes any legal liability or responsibility for the accuracy, completeness, or usefulness of any information, apparatus, product, or process disclosed, or represents that its use would not infringe privately owned rights. Reference herein to any specific commercial product, process, or service by its trade name, trademark, manufacturer, or otherwise, does not necessarily constitute or imply its endorsement, recommendation, or favoring by the United States Government or any agency thereof, or The Regents of the University of California. The views and opinions of authors expressed herein do not necessarily state or reflect those of the United States Government or any agency thereof or The Regents of the University of California and shall not be used for advertising or product endorsement purposes.

Lawrence Berkeley Laboratory is an equal opportunity employer.

This report has been reproduced directly from the  
best available copy.

## **DISCLAIMER**

This document was prepared as an account of work sponsored by the United States Government. While this document is believed to contain correct information, neither the United States Government nor any agency thereof, nor the Regents of the University of California, nor any of their employees, makes any warranty, express or implied, or assumes any legal responsibility for the accuracy, completeness, or usefulness of any information, apparatus, product, or process disclosed, or represents that its use would not infringe privately owned rights. Reference herein to any specific commercial product, process, or service by its trade name, trademark, manufacturer, or otherwise, does not necessarily constitute or imply its endorsement, recommendation, or favoring by the United States Government or any agency thereof, or the Regents of the University of California. The views and opinions of authors expressed herein do not necessarily state or reflect those of the United States Government or any agency thereof or the Regents of the University of California.

**The Dynamics of Electronic to Vibrational, Rotational and Translational  
Energy Transfer in Collision of Ba( $^1P_1$ ) with Diatomic Molecules.**

A. G. Suits\*, P. de Pujo, O. Sublemontier, J.-P. Visticot, J. Berlande,  
J. Cuvellier, T. Gustavsson†, J.-M. Mestdagh‡, and P. Meynadier

*DRECAM/SPAM*

*CEN Saclay*

*91191 Gif-sur-Yvette Cedex, France*

and

Y. T. Lee

*Chemical Sciences Division*

*Lawrence Berkeley Laboratory and*

*Department of Chemistry*

*University of California*

*Berkeley CA 94720*

\*Present address: *Baker Laboratory, Department of Chemistry, Cornell University, Ithaca NY 14853.*

†Present address: *DRECAM/SCM/URA 331 CNRS, CEN/Saclay 91191 Gif-sur-Yvette Cedex,  
France.*

‡Author to whom correspondence should be addressed.

**ABSTRACT**

Doppler measurements taken over a range of probe laser angles in a crossed-beam experiment were used, in conjunction with forward convolution analysis, to obtain flux-velocity contour maps for  $\text{Ba}(^3\text{P}_2)$  produced in collision of  $\text{Ba}(^1\text{P}_1)$  with  $\text{H}_2$ ,  $\text{N}_2$ ,  $\text{O}_2$  and  $\text{NO}$ . The contour maps suggest a general model for the dynamics of this process in which large impact parameter collisions result in a near-resonant transfer of initial electronic energy into final vibrational energy, while close collisions produce sideways scattering and effectively couple electronic energy to translation. The molecular collision partners fall into two categories: for one group, comprising  $\text{O}_2$  and  $\text{NO}$ , the existence of a well-defined molecular anion with favorable Franck-Condon factors linking excited vibrational levels to the ground vibrational state of the neutral results in greatly enhanced coupling for the near-resonant process. Molecules for which there exist no stable anions, such as  $\text{N}_2$  and  $\text{H}_2$ , represent a second category. The electronically inelastic collision for this group is instead dominated by the non-resonant process yielding the ground vibrational state and large translational energy release.

## I. INTRODUCTION

Electronic-to-electronic, vibrational, rotational and translational energy transfer (E→EVRT) represents a central problem in chemical physics whose understanding has important implications for laser physics and atmospheric and combustion chemistry.<sup>1,2</sup> Experimental insights into electronically inelastic collision processes also can provide an important means of exploring the current theoretical understanding of nonadiabatic collision dynamics.<sup>3,4</sup> Quenching of excited electronic states has been studied since the early part of the century, and a large body of data has accumulated concerning total quenching cross sections and relative quenching efficiencies for a broad range of systems.<sup>5</sup> However, experimental results sufficiently detailed to provide insights into the underlying dynamics of these processes have only become possible with the development of laser and molecular beam based techniques.<sup>6,7,8</sup>

In an extensive series of experiments, Hertel and coworkers studied the quenching of electronically excited sodium atoms induced by a variety of molecular collision partners in crossed beams.<sup>8-14</sup> Time-of-flight spectra of superelastically scattered sodium atoms were recorded at a fixed scattering angle and the results allowed inferences to be made about the partitioning of the remaining energy into electronic, vibrational and rotational energy of the molecule. Kwei and coworkers performed complementary studies on the superelastically scattered molecules in some of the same systems, and the broad features of the results from the two groups generally agreed.<sup>15</sup> Owing to the large translational energy release and narrow vibrational distribution inferred for Na(<sup>2</sup>P) quenching by N<sub>2</sub>, Hertel's group studied this system in some detail and their results stimulated considerable theoretical work, notably the ab initio calculations of Habitz.<sup>16,17,18</sup> Ironically, Habitz' calculation showed that it was inappropriate to consider an ionic Na<sup>+</sup>-N<sub>2</sub><sup>-</sup> complex mediating the quenching process, though it was precisely this system for which Bauer, Fisher and Gilmore originally proposed their multi-curve crossing model of E→V energy transfer.<sup>19</sup> Results for quenching by CO and O<sub>2</sub> were quite different from N<sub>2</sub>: the vibrational

distributions were much broader and the translational energy release well described by the statistical prior distribution. For  $O_2$ , however, energy release into translation was relatively small so few conclusions could be drawn.<sup>8</sup>

These experiments, on which rests much of the foundation of our understanding of the dynamics of  $E \rightarrow V$  energy transfer, reveal the inherent difficulties in bringing the full power of crossed beam techniques to bear on inelastic processes involving short-lived excited states. The intrinsic difficulty of obtaining a significant excited state population makes measurements of differential cross sections challenging, and the contribution of background arising from elastic scattering or the beam itself can overwhelm the signal of interest. Furthermore, experiments relying on superelastic scattering are necessarily blind to near-resonant processes in which most of the electronic energy has gone into internal energy of the products. Although not likely to be a significant problem in the sodium studies owing to the large (2.1 eV) available electronic energy, in some cases near-resonant transfer may be the dominant mode of electronic energy release. Finally, if one is interested in  $E \rightarrow EVRT$  energy transfer processes, then some state resolved detection method is necessary in order to distinguish processes yielding the different final electronic states.

One such state-resolved detection method was suggested by the pioneering work of Kinsey, et al., in which Doppler spectroscopy was proposed as a means of obtaining differential cross sections.<sup>20,21,22</sup> Following Kinsey's suggestion, Doppler methods have now been applied to a broad range of problems in chemical dynamics, from atom-atom collisions<sup>23</sup> to vector correlations in photodissociation<sup>24</sup> and even crossed-beam studies of reactive scattering.<sup>25</sup> With one exception<sup>26</sup>, however, Doppler methods have been applied to crossed-beam studies in systems in which the final translational energy is predetermined by conservation of energy given the final detected state, and the probe laser is directed along the relative velocity vector. In that case, the Doppler scans directly yield the differential cross sections. If the final state of the undetected product is not known, then the center-of-mass velocity of the detected product is also unknown



and a range of center-of-mass scattering angles and velocities may satisfy the Doppler resonance condition. By making Doppler measurements at a range of probe laser angles and simulating the results using a forward convolution of assumed forms of the scattering distributions, we have derived doubly differential cross sections for these systems in which the final translational energies were not known. This method has recently been used to reveal Stückelberg oscillations in the differential cross sections for the process  $\text{Ba}(^1\text{P}_1) + \text{Ar} \rightarrow \text{Ba}(^3\text{P}_2) + \text{Ar}$ .<sup>27</sup> In that case since the final translational energy is well known, Doppler scans perpendicular to the beams and along the relative velocity vector are sufficient to constrain the fits.

We applied this method to obtain flux-velocity contour maps for  $\text{Ba}(^3\text{P}_2)$  from collision of  $\text{Ba}(^1\text{P}_1)$  with the diatomic molecules  $\text{O}_2$ ,  $\text{N}_2$ ,  $\text{NO}$  and  $\text{H}_2$ . Two fundamentally different modes of electronically inelastic scattering are observed for different collision partners: one, displayed by  $\text{H}_2$  and  $\text{N}_2$ , results in sideways scattering and large translational energy release; the other, seen in  $\text{O}_2$  and  $\text{NO}$ , results in sharply forward scattering and efficient conversion of initial electronic energy into final vibrational energy. A preliminary report of the results for  $\text{O}_2$  and  $\text{N}_2$  has already appeared.<sup>28</sup>

These studies provide, to our knowledge, the first contour maps obtained for an electronically inelastic scattering process and clearly document a near-resonant process in  $\text{O}_2$ ,  $\text{NO}$  and  $\text{N}_2$ . The results suggest a model for the dynamics of these collisions which invokes the shape of the potential energy surfaces in the crossing regions to account for the observed  $\text{Ba}(^3\text{P}_2)$  scattering distributions. Important differences in the behavior of barium and sodium are also apparent, particularly in the case of collision with  $\text{O}_2$  and  $\text{NO}$ .

## II. EXPERIMENTAL

The experimental apparatus<sup>27,29,30,31</sup> features an effusive barium atomic beam crossed at  $90^\circ$  by a Campargue-type supersonic molecular beam under single collision conditions (Figure 1).

The Ba excitation and detection scheme is summarized in figure 2. The 553.7 nm  $\text{Ba}(^1\text{P}_1 \leftarrow ^1\text{S}_0)$  transition was pumped by a cw single frequency ring dye laser directed through an optic fiber, perpendicular to the collision plane, to the interaction region. Doppler scans of the collisionally populated  $\text{Ba}(^3\text{P}_2)$  state were made by probing the  $\text{Ba}(^3\text{S}_1 \leftarrow ^3\text{P}_2)$  transition at 790.6 nm while monitoring the  $\text{Ba}(^3\text{S}_1 \rightarrow ^3\text{P}_1)$  fluorescence at 739.4 nm. Probe scans were made over a range of about 2 GHz, and a part of the probe laser output was directed into a confocal Fabry-Perot etalon of 300 MHz free spectral range, coupled to a photomultiplier tube. The Fabry-Perot fringes were recorded and later used to linearize the scans. The probe laser power was attenuated by neutral density filters to preclude power broadening of the Ba line. The probe laser was introduced through the same optic fiber as the pump laser for perpendicular scans, or through a second optic fiber in the collision plane for other probe angles. The second fiber could be rotated around the interaction region, allowing for Doppler scans from  $18^\circ$  to  $50^\circ$  from the molecular beam. The relation of the probe laser angle to the laboratory velocity distribution is schematically illustrated in figure 3. The Doppler profiles did not show significant changes when the pump laser polarization was changed; these results were obtained with both pump and probe lasers unpolarized.

Fluorescence from the center of the interaction region ( $\sim 2$  mm) was dispersed by a 0.5 m monochromator of about 5 nm spectral resolution. The monochromator was coupled to an RCA 31034 photomultiplier tube. Filters were used to limit the contribution from  $\text{Ba}(^1\text{P}_1)$  fluorescence ( $10^7$ - $10^9$  times more intense than the signal of interest) as well as the weaker  $\text{Ba}(^3\text{P}_1 \rightarrow ^1\text{S}_0)$  line. In addition, a portion of the light originating in the interaction region was directly sent to another photomultiplier tube to monitor fluorescence from the  $\text{Ba}(^1\text{P}_1)$  state. The latter signal was used to correct for fluctuations in the  $\text{Ba}(^1\text{P}_1)$  population during the course of a scan.

The Doppler scans obtained with the probe laser beam perpendicular to the collision plane are symmetric, so the perpendicular scans are self-calibrating: the center of the scan represents  $\nu_0$ , the unshifted atomic resonance. For the scans obtained with the probe laser in the plane of the

molecular beams, however, it was necessary to refer the recorded spectra to simultaneously measured perpendicular scans to determine the frequency origin. In the earlier experiments this was achieved by alternately recording scans with the probe laser in the plane, then perpendicular to the plane, while ensuring that no mode jumps had occurred in between the scans. In later experiments a moving mirror (1 Hz) was added to direct the probe laser beam alternately into the in-plane and perpendicular optic fibers, while the scaler channel also incremented. This enabled us to record perpendicular scans simultaneously with the in-plane scans, so the origin of each scan was obtained directly.

For the Doppler measurements, all molecular beams except  $H_2$  were seeded in helium. The latter makes no significant contribution to the inelastic process at the collision energies studied.<sup>23</sup> The molecular beam velocities were measured by time of flight using an electron bombardment ionizer-quadrupole mass spectrometer with a chopper wheel. The barium beam velocity distribution was determined by simulation of a Doppler scan taken with the probe laser  $40^\circ$  from the Ba beam on the  $Ba(^1P_1 \rightarrow ^1S_0)$  transition. For the cross section measurements the molecular beam flux was determined by means of a Pitot tube, and the barium beam flux was monitored by means of a quartz balance, as described previously.<sup>29,30,31</sup>

### III. SIMULATION PROGRAM

In the forward convolution<sup>32,33</sup> approach, the Doppler spectra were simulated using a computer program in which assumed forms of the translational energy and angular distributions were used to generate the contribution to the Doppler signal at a given laser angle and frequency offset. The program performed an integration over resonant velocities in the laser reference frame, in which the probe laser direction is taken to be the z axis. The Doppler signal is given by:<sup>34,35,36,37</sup>

$$I(\nu) d\nu = \iiint N(u, \theta_L, \phi_L) \delta(\omega - \vec{V}_{lab} \cdot \hat{n}) u^2 \sin\theta_L du d\theta_L d\phi_L$$

where  $\nu$  is the probe laser frequency,  $u$  is the center of mass speed of the detected particle,  $\vec{V}_{lab}$  is its velocity in the lab frame,  $\theta_L$  and  $\phi_L$  are the center of mass polar and azimuthal angles in the laser reference frame,  $\hat{n}$  is a unit vector in the probe laser direction,  $N(u, \theta_L, \phi_L)$  is the number density distribution of detected particles and  $\omega$  is defined by the Doppler resonance condition:

$$\nu = \nu_0 \left(1 - \frac{\omega}{c}\right)$$

The component of the particle's velocity in the probe laser direction may be expressed in the center of mass frame:

$$\vec{V}_{lab} \cdot \hat{n} = u \cos\theta_L + \vec{V}_{cm} \cdot \hat{n}$$

The Doppler signal, expressed in terms of flux rather than number density,<sup>26</sup> is then given by:

$$I(\nu) = \iiint I(u, \theta_L, \phi_L) \delta(\omega - u \cos\theta_L - \vec{V}_{cm} \cdot \hat{n}) u \sin\theta_L du \frac{d\theta_L}{d\nu} d\phi_L$$

This is the integral performed by the program. The laser reference frame differs from the conventional collision reference frame (in which the relative velocity vector is the z axis) only by a rotation, since they are both center of mass frames. The Jacobian for this transformation is thus unity, and we are free to substitute the flux in the collision reference frame, following the appropriate rotation, for that in the laser reference frame. The flux in the collision reference frame is actually the differential cross section, so we have:

$$I(\nu) = \iiint \frac{d^3\sigma}{d^2\omega du} (u, \theta_L, \phi_L) \delta(\omega - u \cos\theta_L - \vec{V}_{cm} \cdot \hat{n}) u \sin\theta_L du \frac{d\theta_L}{d\nu} d\phi_L$$

This integration is performed at each laser frequency for a given Newton diagram with a weighting determined by measured beam conditions. The process is then repeated for each successive Newton diagram, with ~50 Newton diagrams used in the final fitting. The result is then convoluted over a 50 MHz Lorentzian to account for power broadening, found to give consistent results for all the systems studied.

The differential cross sections are generated from assumed forms of the translational energy and angular distributions. Independent translational energy and angular distributions were assumed for each final vibrational state of the molecular collision partner, with the contributions summed to give the simulated spectra. Although some of the data could be fitted with a single separable angular and translational energy distribution, the result was artificial: for N<sub>2</sub>, for example, a small, sharp forward scattered peak was constrained by the dominant sideways scattering to appear with large translational energy release. The final vibrational states were thus fitted separately in order to obtain physically reasonable distributions. The sensitivity of the fits to the contribution of each final vibrational state varied considerably with the nature of the scattering distribution, so this will be indicated in the Results section.

## IV. RESULTS

### A. H<sub>2</sub>

Doppler spectra of Ba(<sup>3</sup>P<sub>2</sub>) from collision of Ba(<sup>1</sup>P<sub>1</sub>) with H<sub>2</sub> at a nominal collision energy of 0.17 eV are shown in figure 4, along with fits obtained as described. Owing to the unfavorable kinematics in this case the scattered Ba(<sup>3</sup>P<sub>2</sub>) center of mass velocity is small, so the Doppler scans are compressed. Nevertheless, a pronounced dip is apparent in the perpendicular scan, indicating large translational energy release and sideways scattering. The results obtained for probe laser

angles in the plane of the beams further constrain the fit and provide enhanced resolution at complementary regions of the scattering distribution.<sup>22</sup>

The fit for  $\text{H}_2$  includes no contribution from vibrationally excited products: the large translational energy release precludes any significant population of  $\text{H}_2$  ( $v=1$ ). The  $\text{Ba}(^3\text{P}_2)$  flux-velocity contour map obtained from the fit is shown superimposed on the most probable Newton diagram in figure 5. The shape of the Doppler scans for the in-plane probe laser angles are sensitive to the location and width of the peak of the angular distribution in this case, so the sharp scattering somewhat forward of  $90^\circ$  is unambiguous. The  $\text{H}_2$  fits are less sensitive to the details of the energy release however, so that it would be difficult to estimate the extent of rotational excitation.

## B. $\text{O}_2$

Figure 6 shows Doppler scans of  $\text{Ba}(^3\text{P}_2)$  produced in collision of  $\text{Ba}(^1\text{P}_1)$  with  $\text{O}_2$  at 0.21 eV. The sharp, narrow perpendicular scan indicates either very low translational energy release or scattering toward the poles. Results for in-plane probe laser angles confirm that the distribution is sharply forward scattered with low translational energy release. The fits include 65% contribution from  $v=3$  and 35% from  $v=2$ .

The contour map of scattered  $\text{Ba}(^3\text{P}_2)$  flux obtained from the fit, shown in figure 7, reveals a striking feature of this distribution: the peak appears very nearly at the tip of the velocity vector of the incident barium beam. This sharp peak corresponds to production of  $\text{O}_2$  ( $v=3$ ). As can be seen more clearly in the inset surface plot, the  $v=2$  component, representing somewhat larger translational energy release, includes a much broader angular distribution. The relative contributions of these two channels are also indicated in each of the Doppler scans in figure 6. There is no indication of any component containing sufficient translational energy to correspond to  $\text{O}_2$  ( $v=0$  or  $1$ ). The fit in this case is not very sensitive to the relative contributions

of  $v=2$  and  $v=3$  ( $\pm 10\%$ ) if the angular distributions are also adjusted, but the sharp peak near the  $v=3$  limit dominates every fit. Owing to an error in the fitting procedure, the vibrational composition of these fits was previously reported<sup>28</sup> as 80% ( $v=3$ ) and 20% ( $v=2$ ) rather than 65% ( $v=3$ ) and 35% ( $v=2$ ).

### C. $N_2$

Results for  $N_2$  at a collision energy of  $0.2\bar{1}$  eV are shown in figure 8 along with fits that include significant contributions from  $v=0, 1$  and  $2$ . The broad perpendicular scan indicates substantial translational energy release and sideways scattering as in the case of  $H_2$ . Yet in place of the central dip we now see a small sharp peak reminiscent of the  $O_2$  distribution. The results for in-plane probe laser angles reveal that this peak must originate from sharply forward scattered  $Ba(^3P_2)$  as in the case of  $O_2$ . Because this sharp forward peak actually represents only a small fraction of the total flux, the fit is not sensitive to the translational energy release accorded this channel. Guided by the  $O_2$  results, however, and using  $N_2$   $v=2$  as the near-resonant channel, we obtain the contour map shown in figure 9.

The inset surface plot in figure 9 shows the contribution from  $v=1$  more clearly. The relative contributions are indicated in table 1, and their contributions to the total fit are also displayed in figure 8. Owing to the  $\sin(\theta)$  weighting of the distribution when integrated over the 3 dimensional scattering volume, the sharp forward scattered  $v=2$  component represents only 6% of the total scattered  $Ba(^3P_2)$  flux, despite its prominence in the contour map.

#### D. NO

The NO results shown in figure 10 strongly resemble the O<sub>2</sub> results in figure 6. The distribution is clearly dominated by sharply forward scattered Ba(<sup>3</sup>P<sub>2</sub>) with low translational energy release. The width of the peak in the perpendicular case, however, and the in-plane scans show evidence for somewhat larger translational energy release and a broader angular distribution for NO than is seen in O<sub>2</sub>.

This is more readily apparent in a comparison of the inferred flux distributions for O<sub>2</sub> and NO shown in figures 7 and 11, respectively. The fit for NO includes contributions from v=0 as well as the dominant v=2 and v=1. Furthermore, the surface plot reveals significant backscattering included in the v=1 angular distribution. This was necessary to fit the in-plane scans; backscattering included in the v=2 channel did not have sufficient translational energy to reproduce the measured distributions. Only a small amount of v=0 was necessary to fit the wings of the Doppler scans. The relative intensities of the different channels are summarized in table I.

Just as in the case of O<sub>2</sub>, these fits are very sensitive to the relative contribution of the sharp near-resonant peak and the broader, larger translational energy component. The fit is not as sensitive to the details of the low intensity components, so corresponding adjustment of the angular distributions would enable a range of translational energy distributions to provide adequate fits.

#### E. Total Ba(<sup>3</sup>P<sub>2</sub>) cross sections

Total cross sections for the process Ba(<sup>1</sup>P<sub>1</sub>) + M → Ba(<sup>3</sup>P<sub>2</sub>) + M are presented in figure 12. Results for the rare gases from reference 23 are included to facilitate the discussion. For NO and H<sub>2</sub>, measurements were made only at the indicated collision energy. The indicated energies are "most probable" collision energies; no attempt has been made to deconvolute the spread resulting



from the spread in beam velocities. The results for the rare gases reveal the presence of a small barrier to the curve crossing as has been discussed elsewhere.<sup>23,38</sup> Except for H<sub>2</sub>, the molecular collision partners show substantially larger cross sections for this process, reaching 26 Å<sup>2</sup> for NO. The steepness of the drop in the cross section with collision energy for N<sub>2</sub> is probably underestimated owing to the spread in the beam velocities. O<sub>2</sub> shows a reverse trend and is still increasing significantly at the highest collision energy measured.

## V. DISCUSSION

The dynamics of related atom-atom collisions have been studied in some detail, and they provide a useful starting point for discussion of these more complex systems. Breckenridge and Merrow<sup>38</sup> found that thermal energy collision of Ba(<sup>1</sup>P<sub>1</sub>) with rare gases results exclusively in production of Ba(<sup>3</sup>P<sub>2</sub>) and ascribed this to inefficient or inaccessible crossings of the weakly attractive Ba(<sup>1</sup>P<sub>1</sub>)-RG (<sup>1</sup>Π) and repulsive Ba(<sup>3</sup>P<sub>1,0</sub>)-RG (<sup>3</sup>Π) curves. Subsequent crossed-beam studies confirmed the existence of a barrier for the production of Ba(<sup>3</sup>P<sub>1</sub>) in Ba(<sup>1</sup>P<sub>1</sub>) collision with Ar, and this was attributed to the location of the crossing on the repulsive wall of the Ba(<sup>1</sup>P<sub>1</sub>)-Ar (<sup>1</sup>Π) curve.<sup>23</sup>

The dynamics of these atom-diatom collisions also be considered in view of the location of crossings of the relevant potential energy surfaces and the shape of the surfaces in these crossing regions. Figure 13 shows a series of curves for Ba(<sup>1</sup>P<sub>1</sub>)-N<sub>2</sub> and Ba(<sup>3</sup>P<sub>2</sub>)-N<sub>2</sub> from reference 39 obtained using the approach described by Hickman<sup>40</sup> for alkali metal(np <sup>2</sup>P)-H<sub>2</sub>, N<sub>2</sub> systems. These curves represent an average over N<sub>2</sub> orientation in C<sub>s</sub> geometry, hence are of either A' or A'' symmetry, although for clarity only the A'' curves are displayed in figure 13. Curves representing the different final N<sub>2</sub> vibrational states were obtained by simply shifting the ground state Ba(<sup>3</sup>P<sub>2</sub>)-N<sub>2</sub> curves by the appropriate N<sub>2</sub> vibrational frequency. The curves so obtained are

adequate for use in locating the crossing regions and in order to sketch a model of the underlying dynamics despite the attendant oversimplification.

This spin changing collision process is allowed, between states of the same symmetry, as a consequence of the large spin-orbit coupling of barium. The crossing regions responsible for this process are indicated by circles in figure 13 for each final  $N_2$  vibrational state. Similar crossings are exhibited by the  $A'$  curves that are not shown. For a collision system approaching on the  $Ba(^1P_1)-N_2$  ( $v=0$ ) curve, the first encounter with a set of triplet curves is with  $Ba(^3P_2)-N_2$  ( $v=2$ ). This occurs with very unfavorable Franck-Condon factors so the coupling is expected to be weak. Furthermore, these crossings are in a flat region of the potential hence little deflection is expected for these trajectories. The  $v=1$  triplet curves are next encountered, and they will possess more favorable Franck-Condon factors than the  $v=2$  curves, resulting in stronger coupling at these crossings.  $Ba(^3P_2)$  flux originating here will descend the repulsive triplet curves, so more deflection is anticipated for the  $Ba(^3P_2)$  corresponding to  $N_2$  ( $v=1$ ) than ( $v=2$ ). Coupling to the  $v=0$  triplet curves will, of course, have the most favorable Franck-Condon factors. In addition, this inner crossing region leads to a long descent on steeply repulsive triplet curves, so the greatest deflection as well as the greatest flux is expected to accompany  $N_2$  ( $v=0$ ).

The model sketched above reproduces all the essential features of the distribution shown in figure 9: the dominant channel is that leading to  $N_2$  ( $v=0$ ), with substantial sideways scattering;  $N_2$  ( $v=1$ ) and ( $v=2$ ) correspond to successively smaller fractions of the observed flux and the  $N_2$  ( $v=2$ ) component shows the sharp forward scattering expected for trajectories experiencing only the flat region of the potential.

This sharply forward scattered  $v=2$  component represents a near-resonant energy transfer from initial  $Ba(^1P_1)$  electronic energy to final  $N_2$  vibration, with little attendant momentum transfer. These near-resonant processes are likely the result of large impact parameter collisions; close collisions will encounter the repulsive wall inevitably resulting in some momentum transfer and greater deflection. The greater statistical weight afforded the large impact parameter

collisions suggests that the near-resonant process might dominate, depending on the strength of the coupling and competition with other exit channels. The fact that it is so weak in the case of  $N_2$  indicates that the coupling is indeed very inefficient. The sensitivity of the technique to this near-resonant process demonstrates the virtue of this state-resolved detection for these experiments: this component is actually superimposed on the barium beam itself, which, although many orders of magnitude more intense, contributes no background to the signal of interest.

The earlier  $Na(^2P)-N_2$  studies provide a useful comparison to the results obtained here. The ionization potential of  $Na(3^2P)$  and  $Ba(6^1P_1)$  are nearly identical ( $\sim 3$  eV) but for sodium, quenching to the ground state is the only available electronically inelastic channel. Habitz showed that although the  $Na-N_2$  ground and excited state surfaces do not cross in an energetically accessible region for  $N_2$  fixed at its equilibrium bond length, prestretching of the  $N_2$  bond on the adiabatic surface brings the crossing seam lower in energy.<sup>16</sup> This prestretching is important both in that it allows the quenching to occur and it facilitates the production of vibrationally excited  $N_2$ . Because the two electronic states of interest in the barium case are so much closer together, the crossings generally occur in the attractive region of the upper surface and prestretching is not a prerequisite for the electronic transition. Nevertheless prestretching is likely to occur, and the production of vibrationally excited  $N_2$  is probably a consequence of this. Although the resolution of the experiment is inadequate to make strong assertions concerning the extent of rotational excitation of  $N_2$ , the fit implies  $\sim 0.1$  eV in rotational energy for the ground vibrational state  $N_2$ , consistent with the substantial rotational excitation anticipated from a close collision.

The results for  $H_2$  are quite reminiscent of the  $v=0$  channel in  $N_2$ . The  $Ba(^3P_2)$  distribution is strongly sideways scattered resulting in the characteristic shape of the perpendicular Doppler profile in figure 4. Unlike the  $N_2$  results, however, the  $H_2$  shows no sign of the forward scattered near-resonant component. For  $H_2$ ,  $v=1$  is the only accessible vibrationally excited state, yet it is far from resonant. From the model sketched above, we would anticipate greater deflection to accompany these trajectories, perhaps resembling the  $v=1$

component of the  $N_2$  distribution more than the  $v=2$  component. Because the  $H_2$  Doppler scans are kinematically compressed, the fits are not sufficiently sensitive to exclude the possibility of 10%  $v=1$ , if its angular distribution were to resemble that indicated for  $v=0$ .

The results for  $O_2$  and NO appear to be fundamentally different from the  $N_2$  and  $H_2$  distributions. In contrast to the dominant  $v=0$ , sideways scattering seen for the latter molecules, NO and  $O_2$  both show near-resonant energy transfer and sharp forward scattering as the primary mode of transition to  $Ba(^3P_2)$ . The differences are readily seen in table I, where the fraction accorded each final vibrational state is indicated. For both NO and  $O_2$ , the near-resonant channel accounts for ~65% of the flux, while for  $N_2$  and  $H_2$  it is ~6% and ~0% respectively. What can account for the dramatically different behavior of these two pairs of molecules? From the model sketched above we infer that the coupling at the first encountered crossing is much stronger for  $O_2$  and NO, but what is the origin of this enhanced coupling? Previous work has shown that a picture of the Na- $N_2$  quenching process involving an ionic intermediate is inappropriate, and the same view was implicit in the discussion of the  $N_2$  and  $H_2$  results.  $N_2$  and  $H_2$  both possess negative "electron affinities", i.e., broad shape resonances in electron scattering at ~2.3 and ~3 eV respectively.<sup>41</sup> These resonances imply the existence of short-lived compound states well above the energy of the neutral molecules.  $O_2$  and NO, however, both possess positive electron affinities (adiabatic values of 0.43 and 0.024 eV respectively);  $O_2^-$  is actually bound for  $v=3$  and below, and  $NO^-$  ( $v=0$ ) is likewise stable. An examination of the  $O_2/O_2^-$  and  $NO/NO^-$  potential energy curves<sup>41</sup> proves more useful than a consideration of the adiabatic electron affinities alone, however. In both cases the vertical electron affinities are slightly negative (roughly -0.6 for  $O_2$  and -0.4 eV for NO), but possess favorable Franck-Condon factors between the ground vibrational state of the neutrals and excited vibrational states of the negative ions. The different dynamics displayed by  $O_2$  and NO on one hand, and  $H_2$  and  $N_2$  on the other, may again be understood with reference to the relevant potential curves. Figure 14 shows a sketch of these curves for the Ba- $O_2$  system. These are roughly represented as flat covalent curves and a  $1/r$

Coulombic curve, shifted by the appropriate energies for the states indicated. The ionic curve indicated ( $O_2^-, v=3$ ) is that consistent with a vertical transition. The strong coupling that may exist between the ionic curve and the various covalent curves serves to enhance coupling among the latter. The crucial difference between these two categories of quenching molecules is thus the existence of well-defined, vibrationally excited states of the negative molecular ions at relatively low energies, which serve to conduct the initial electronic energy very efficiently into nuclear motion. Similar observations were made by Breckenridge and Umemoto<sup>2</sup> to explain the differences in quenching efficiencies of  $Hg(^3P_0)$  by NO and CO.<sup>6</sup> This inelastic transition for  $O_2$  and NO thus should be well suited for theoretical treatment via the multi-curve crossing approach.<sup>42</sup>

The Na( $3^2P$ ) quenching results again provide an interesting contrast to those obtained here. The crossed-beam studies of Kwei and coworkers<sup>15</sup> for quenching by NO indicate a collision complex surviving longer than a rotational period, inferred from the characteristic symmetric scattering along the poles. This is consistent with a strong NaNO ionic bond implied in recent Na-NO<sub>2</sub> reactive scattering experiments.<sup>43</sup> The final NO vibrational distribution in the sodium quenching studies thus more closely resembles a statistical distribution characterized by the total available energy, with the initial impact parameter likely to show little correlation to the final vibrational state.

The parallel exhibited by NO and  $O_2$  in the dynamics of the Ba( $1^1P_1$ ) inelastic scattering process is surprising. Collision of both ground state and electronically excited Ba with  $O_2$  appears to be dominated by the production of BaO, with a very large cross section for this process. Collision of ground state Ba with  $O_2$  clearly shows the existence of a stable BaO<sub>2</sub> collision complex, the consequence of a strong BaO<sub>2</sub> ionic bond just as in the case of NaNO.<sup>45,44</sup> But the existence of the exoergic reactive channel drains the complexes away from other possible exit channels. Studies of chemiluminescence from the electronically excited BaO produced in reaction of Ba( $1^1D$ ) and Ba( $1^1P$ ) with  $O_2$  indicate that in the former case the BaO\* appears to show a

statistical distribution of final vibrational states, while in the latter case the final vibrational distribution is clearly non-statistical,<sup>45</sup> and a direct mechanism was proposed to account for this observation. Yet recent experiments at Berkeley that do not resolve the final electronic state suggest that the collision complex is still important even for reaction of Ba(<sup>1</sup>P<sub>1</sub>), perhaps yielding ground state rather than electronically excited BaO.<sup>47, 48</sup> Small impact parameter collisions of Ba(<sup>1</sup>P<sub>1</sub>) with O<sub>2</sub> thus probably lead to a closely coupled BaO<sub>2</sub> intermediate that produces reactive BaO product, rarely leading to Ba(<sup>3</sup>P<sub>2</sub>).

Reaction of ground state Ba with NO to yield BaO is actually endoergic, however, owing to the strength of the NO bond. Studies of this system at Berkeley indicate that for the ground state the dominant collision processes are non-reactive, again through a long-lived complex. BaNO has recently been observed from reaction of Ba with NO<sub>2</sub> and a bond energy of 65 kcal/mole obtained from the maximum translational energy release in that reaction.<sup>43</sup> Again the strong BaNO bond accounts for the existence of a long-lived collision complex. A small yield of BaO is observed at high collision energies or from reaction of Ba(<sup>1</sup>P), yet even in this case inelastic processes dominate over reactive scattering.<sup>48</sup> There is thus an important difference between the Ba(<sup>1</sup>P<sub>1</sub>)-O<sub>2</sub> and Ba(<sup>1</sup>P<sub>1</sub>)-NO collision dynamics. In the former case, the strongly exoergic reactive channel drains flux away from inelastic channels, while for the latter system inelastic scattering dominates even though reaction is energetically possible. Yet in both cases the distribution of Ba(<sup>3</sup>P<sub>2</sub>) is very similar. This suggests that for both these systems it is only the large impact parameter collisions that lead to Ba(<sup>3</sup>P<sub>2</sub>); small impact parameter collisions that sample the full depth of the attractive well have little probability of exiting as Ba(<sup>3</sup>P<sub>2</sub>), instead resulting in orbiting collisions. For O<sub>2</sub> this yields BaO with a high probability, while for NO the dominant product is probably ground state Ba and vibrationally excited NO. The Ba(<sup>3</sup>P<sub>2</sub>) distribution from collision with NO actually shows some backscattering in the NO(v=1) channel, seen clearly in the surface plot of figure 11. This could result from orbiting collisions which occasionally yield

Ba( $^3P_2$ ). The absence of any similar backscattering from O<sub>2</sub> may be attributed to the dominant reactive channel in that case.

The cross sections in figure 12 reveal another important difference between O<sub>2</sub> and NO: the cross section for the latter process is approximately double that of the former. Again, the existence of a dominant reactive channel for O<sub>2</sub> may account for this difference. The nonstatistical electronically excited BaO produced in reaction of Ba( $^1P_1$ ) with O<sub>2</sub> might be the result of large impact parameter collisions. This could produce BaO\* directly, much as has been suggested to account for BaO\* from the ground state reaction with NO<sub>2</sub>.<sup>43</sup> Electron transfer to O<sub>2</sub> will initiate stretching of the (O-O)<sup>-</sup> bond in the familiar "harpoon mechanism", with dissociation of O<sub>2</sub><sup>-</sup> ultimately yielding BaO + O. The energy dependence seen in the cross section for O<sub>2</sub> is also consistent with this picture. At higher collision energies, the O<sub>2</sub><sup>-</sup> has less time to stretch, so reverse electron transfer and exit on one of the neutral nonreactive surfaces is more likely. Such behavior has been amply demonstrated in a variety of electron transfer reactions.<sup>23</sup> The larger cross section for the inelastic process for NO may thus be owing to the absence of a readily available reactive path from large impact parameter collisions.

The sharp initial drop in the N<sub>2</sub> cross section in figure 12 is quite interesting. The prestretching phenomenon suggested above to account for the near-resonant process in N<sub>2</sub> predicts a decreasing cross section with increasing collision energy, but would not anticipate the sudden, dramatic drop seen in figure 12. More likely there exists a barrier to some competing process (such as the production of Ba( $^3P_{1,0}$ )), so the drop in Ba( $^3P_2$ ) production might actually reflect a dramatic change in branching to the competing channel. Unfortunately interference from neighboring Ba lines makes it impossible for us to study the Ba( $^3P_{1,0}$ ) channels.

## VI. CONCLUSION

The use of state-resolved Doppler measurements over a range of probe laser angles in crossed-beam experiments, in conjunction with a forward convolution analysis, provides a powerful technique for the study of inelastic collision processes. This technique enabled us to

obtain flux-velocity contour maps for  $\text{Ba}(^3\text{P}_2)$  from collision of  $\text{Ba}(^1\text{P}_1)$  with a variety of diatomic molecules. The contour maps suggest a general model for the collision dynamics of this process in which large impact parameter collisions result in a near-resonant transfer of initial electronic energy into final vibrational energy while close collisions produce sideways scattering and effectively couple electronic energy to translation. The molecular collision partners fall into two categories: the existence of a stable molecular anion with favorable Franck-Condon factors can result in greatly enhanced coupling for the near-resonant process, exemplified by  $\text{O}_2$  and  $\text{NO}$ , while molecules for which there exist no stable anions, such as  $\text{H}_2$  and  $\text{N}_2$ , will be dominated by non-resonant quenching yielding the ground vibrational state and large translational energy release.

#### **Acknowledgement**

This work was supported by NATO Grant 99/89, and the Director, Office of Energy Research, Office of Basic Energy Sciences, Chemical Sciences Division, of the U.S. Department of Energy under Contract No. DE-AC03-76SF00098. AGS acknowledges Dr. H. F. Davis for helpful discussions, and the NSF for a graduate fellowship.



## REFERENCES

1. I. V. Hertel, *Adv. Chem. Phys.* **45**, 341 (1981).
2. W. H. Breckenridge and H. Umemoto, in *The Dynamics of the Excited State*, K. P. Lawley, ed., *Adv. Chem. Phys.* **50**, (Wiley, New York, 1982).
3. M. Baer, in *Molecular Collision Dynamics*, J. M. Bowman, ed., p. 117 (Springer-Verlag, New York, 1983).
4. A. Sevin, C. Giessner-Prettre, P. C. Hiberty and E. Noizet, *J. Phys. Chem.*, **95**, 8580 (1991).
5. L. Krause, *Adv. Chem. Phys.* **48**, 267 (1975) and references.
6. H. Horiguchi and S. Tsuchiya, *J. Chem. Phys.* **70**, 762 (1979).
7. J. Degani, E. Rosenfeld and S. Yatsiv, *J. Chem. Phys.* **68**, 4041 (1978).
8. I. V. Hertel, *Adv. Chem. Phys.* **50**, 456 (1982).
9. E. E. B. Campbell, H. Schmidt and I. V. Hertel, *Adv. Chem. Phys.* **72**, 37 (1988).
10. I. V. Hertel, H. Hoffmann and K. A. Rost, *Phys. Rev. Lett.*, **36**, 861 (1976).
11. I. V. Hertel, H. Hoffmann and K. A. Rost, *Chem. Phys. Lett.*, **47**, 163 (1977).
12. I. V. Hertel, H. Hoffmann and K. A. Rost, *J. Chem. Phys.*, **71**, 674 (1979).
13. I. V. Hertel and W. Reiland, *J. Chem. Phys.*, **74**, 6757 (1981).
14. G. Jamieson, W. Reiland, C. P. Schultz, H. U. Tittes and I. V. Hertel, *J. Chem. Phys.*, **81**, 5805 (1984).
15. J. A. Silver, N. C. Blais and G. H. Kwei, *J. Chem. Phys.* **71**, 3413 (1979).
16. P. Habitz, *Chem. Phys.*, **54**, 131 (1980).
17. P. Achirel and P. Habitz, *Chem. Phys.*, **78** 213 (1983).
18. D. Poppe, D. Papierowska-Kaminski, V. Bonacic-Koutecky, *J. Chem. Phys.*, **86**, 822 (1987).
19. E. Bauer, E. R. Fisher and F. R. Gilmore, *J. Chem. Phys.*, **51**, 4173 (1969).
20. J. L. Kinsey, *J. Chem. Phys.* **66**, 2560 (1976).

21. W. D. Phillips, J. A. Serri, D. J. Ely, D. E. Pritchard, K. R. Way and J. L. Kinsey, *Phys. Rev. Lett.*, **41**, 937 (1978).
22. J. A. Serri, J. L. Kinsey and D. E. Pritchard, *J. Chem. Phys.* **75**, 663 (1981).
23. J. P. Visticot, J. Berlande, J. Cuvelier, J.M. Mestdagh, P. Meynadier, P. de Pujo, O. Sublemontier, A. Bell and J. Frey, *J. Chem. Phys.* **93**, 5354 (1990).
24. P. L. Houston, *J. Phys. Chem.*, **91**, 5388 (1987).
25. B. Girard, N. Billy, G. Gouedard and J. Vigue, *Europhysics Lett.* **14**, 13 (1991).
26. E. L. Murphy, J. H. Brophy, G. S. Arnold, W. L. Dimpfl and J. L. Kinsey, *J. Chem. Phys.* **70**, 5910 (1979).
27. J.-P. Visticot, P. de Pujo, O. Sublemontier, A. J. Bell, J. Berlande, J. Cuvelier, T. Gustavsson, A. Lallement, J.-M. Mestdagh, P. Meynadier and A. G. Suits, *Phys. Rev. A* **45** (1992).
28. A. G. Suits, P. de Pujo, O. Sublemontier, J.-P. Visticot, J. Berlande, J. Cuvelier, T. Gustavsson, J.-M. Mestdagh, P. Meynadier and Y. T. Lee, *Phys. Rev. Lett.*, **67**, 3070 (1991).
29. J. Cuvelier, J. M. Mestdagh, J. Berlande, P. de Pujo, and A. Binet, *Rev. Phys. Appl.* **16**, 679, (1981).
30. J. Cuvelier, P. de Pujo, J. M. Mestdagh, J. P. Visticot, J. Berlande and A. Binet, *J. Chem. Phys.* **90**, 7050 (1989).
31. J. M. Mestdagh, J. Berlande, J. Cuvelier, P. de Pujo and A. Binet, *J. Phys. B* **15**, 439 (1982).
32. E. Entemann, *J. Chem. Phys.* **55**, 4872 (1971).
33. R. Buss, Ph.D. Thesis, Univ. of Calif., Berkeley, (1972).
34. R. Schmiedl, H. Dugan, W. Meier and K. H. Welge, *Z. Phys. A* **304**, 137 (1982).
35. R. N. Dixon, *J. Chem. Phys.* **85**, 1866 (1986).
36. N. Kouchi, K. Ito, Y. Hatano and N. Oda, *Chem. Phys.* **70**, 105 (1982).

37. R. Vasudev, R. N. Zare and R. N. Dixon, *J. Chem. Phys.* **80**, 4863 (1984).
38. W. H. Breckenridge and C. N. Merrow, *J. Chem. Phys.* **88**, 2329 (1988).
39. J.-M. Mestdagh, P. Meynadier, P. de Pujo, O. Sublemontier, J.-P. Visticot, J. Berlande, J. Cuvellier, T. Gustavsson, A. G. Suits and Y. T. Lee, submitted to *Physical Review A*.
40. A. P. Hickman, *J. Phys. B* **15**, 3005 (1982).
41. G. J. Schulz, *Rev. Mod. Phys.*, **45**, 423 (1973).
42. D. Paillard and J.-M. Mestdagh, *J. Chem. Phys.*, **91**, 6866 (1989).
43. H. F. Davis, A. G. Suits and Y. T. Lee, *J. Chem. Phys.* in press.
44. H. F. Davis, A. G. Suits and Y. T. Lee, *Ber. Bunsenges. Phys. Chem.* **94**, 1193 (1990).
45. J.-P. Visticot, C. Alcaraz, J. Berlande, J. Cuvellier, T. Gustavsson, J.-M. Mestdagh, P. Meynadier, P. de Pujo and O. Sublemontier, *J. Chem. Phys.*, **94**, 4913 (1990).
46. J.-M. Mestdagh, P. Meynadier, P. de Pujo, O. Sublemontier, J.-P. Visticot, C. Alcaraz, J. Berlande and J. Cuvellier, *Chem. Phys. Lett.*, **164**, 5 (1989).
47. H. F. Davis, A. G. Suits, Y. T. Lee, C. Alvarez and J.-M. Mestdagh, unpublished results.
48. H. F. Davis, A. G. Suits and Y. T. Lee, unpublished results.
49. J. Los and A. W. Kleyn, in *Alkali Halide Vapors*, 189 (Academic Press, New York, 1979) and references.

	H <sub>2</sub>	N <sub>2</sub>	NO	O <sub>2</sub>
v=0	100%	80	6	
v=1	0*	14	29	
v=2		6*	65*	35
v=3				65*

Table 1. Relative contribution for each vibrational state used in the fits shown in figures 4 to 11.

Asterisk indicates near-resonant channel.

### Figure Captions

1. Schematic representation of crossed-beam apparatus.
2. Barium energy diagram illustrating the excitation and detection scheme.
3. Schematic illustration of Doppler technique showing relation between laboratory and center-of-mass velocity space and probe laser directions. Dotted lines indicate regions of zero frequency offset for corresponding orthogonal probe laser direction. In addition to the indicated probe laser angles, scans were also obtained with the probe laser perpendicular to the plane defined by the figure.
4. Doppler scans of  $\text{Ba}(^3\text{P}_2)$  produced from collision of  $\text{Ba}(^1\text{P}_1)$  with  $\text{H}_2$  at 0.17 eV collision energy taken at the indicated probe laser angles. The circles are experimentally measured; the lines are best-fit simulations.
5. Velocity space  $\text{Ba}(^3\text{P}_2)$  flux contour map obtained from the fit shown in Figure 4 for collision of  $\text{Ba}(^1\text{P}_1)$  with  $\text{H}_2$ . The inset shows the same data presented as a surface plot.
6. Doppler scans of  $\text{Ba}(^3\text{P}_2)$  produced from collision of  $\text{Ba}(^1\text{P}_1)$  with  $\text{O}_2$  at 0.21 eV collision energy taken at the indicated probe laser angles.  
The circles are experimentally measured; lines are best-fit simulations. ---- Total fit; .-. .- v=2; .....v=3.
7. Contour map of  $\text{Ba}(^3\text{P}_2)$  flux obtained from the fit shown in Figure 6 for collision of  $\text{Ba}(^1\text{P}_1)$  with  $\text{O}_2$ . Near resonant (v=3) channel has been reduced 5-fold.
8. Doppler scans of  $\text{Ba}(^3\text{P}_2)$  produced from collision of  $\text{Ba}(^1\text{P}_1)$  with  $\text{N}_2$  at 0.21 eV collision energy obtained at the indicated probe laser angles. The circles are experimentally measured; lines are best-fit simulations. ---- Total fit; ..-..-..- v=0; .-.-. v=1; .... v=2.
9. Contour map of  $\text{Ba}(^3\text{P}_2)$  flux obtained from the fit shown in Figure 8 for collision of  $\text{Ba}(^1\text{P}_1)$  with  $\text{N}_2$ . Near resonant (v=2) channel has been reduced 5-fold.

10. Doppler scans of  $\text{Ba}(^3\text{P}_2)$  produced from collision of  $\text{Ba}(^1\text{P}_1)$  with NO at 0.21 eV collision energy obtained at the indicated probe laser angles. The circles are experimentally measured; lines are best-fit simulations. ---- Total fit; ...-.-.- v=0; .-.-.- v=1; .... v=2.
11. Contour map of  $\text{Ba}(^3\text{P}_2)$  flux obtained from the fit shown in Figure 10 for collision of  $\text{Ba}(^1\text{P}_1)$  with NO. Near resonant (v=2) channel has been reduced 5-fold.
12. Energy dependence of the  $\text{Ba}(^1\text{P}_1) + \text{M} \rightarrow \text{Ba}(^3\text{P}_2) + \text{M}$  cross section where M is indicated rare gas atom or diatomic molecule.
13. Ba-N<sub>2</sub> potential energy curves of A' symmetry correlating to 6s6p <sup>1,3</sup>P states of Ba, for indicated N<sub>2</sub> vibrational level.
14. Schematic representation of Ba-O<sub>2</sub> potential curves for the indicated Ba electronic states and O<sub>2</sub> vibrational level.

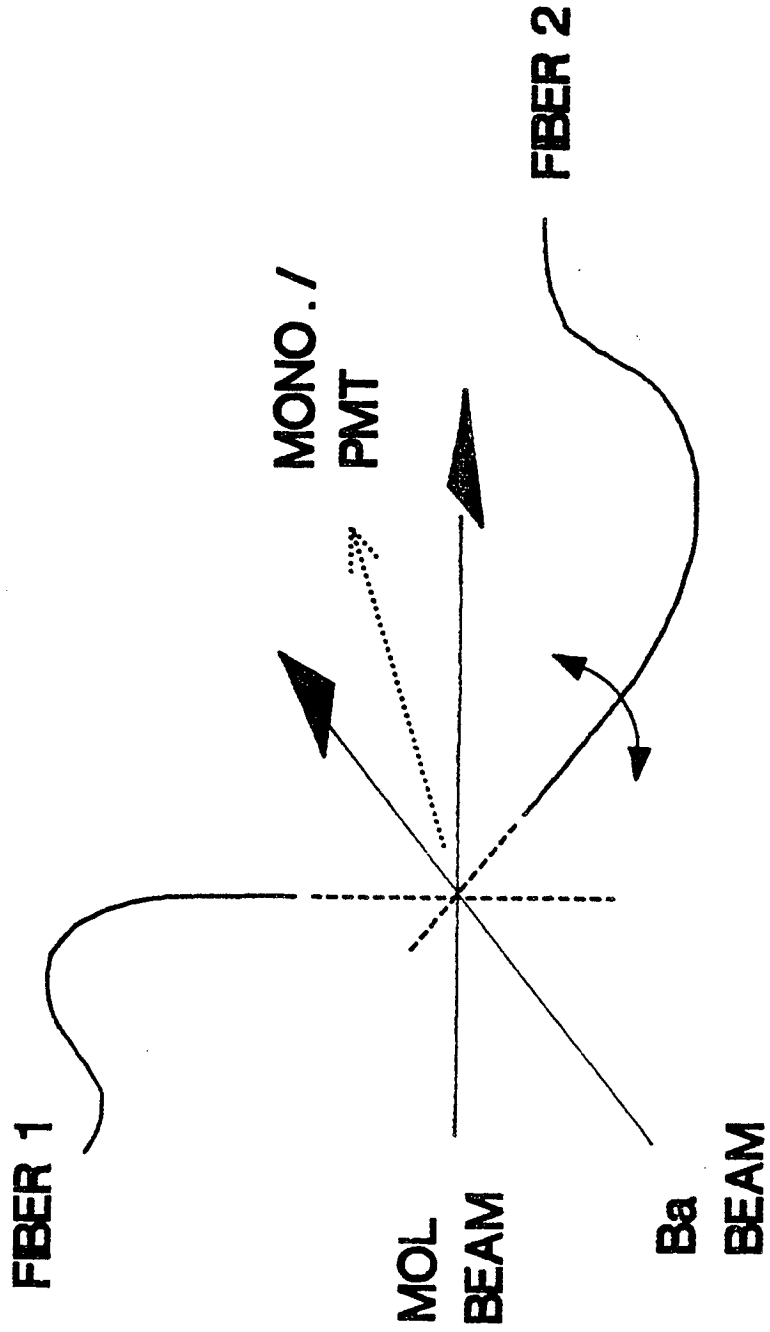


Fig. 1

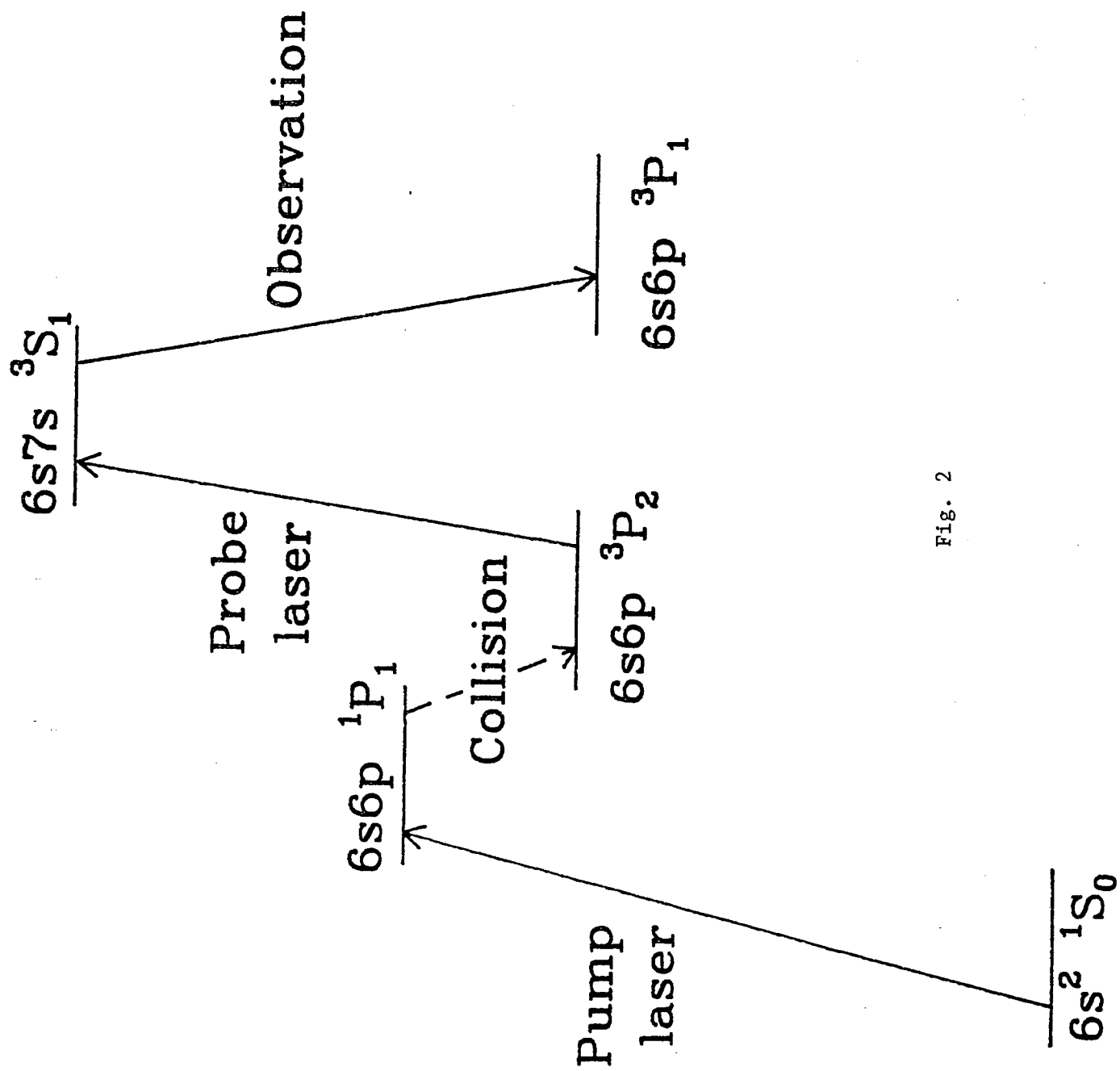


Fig. 2



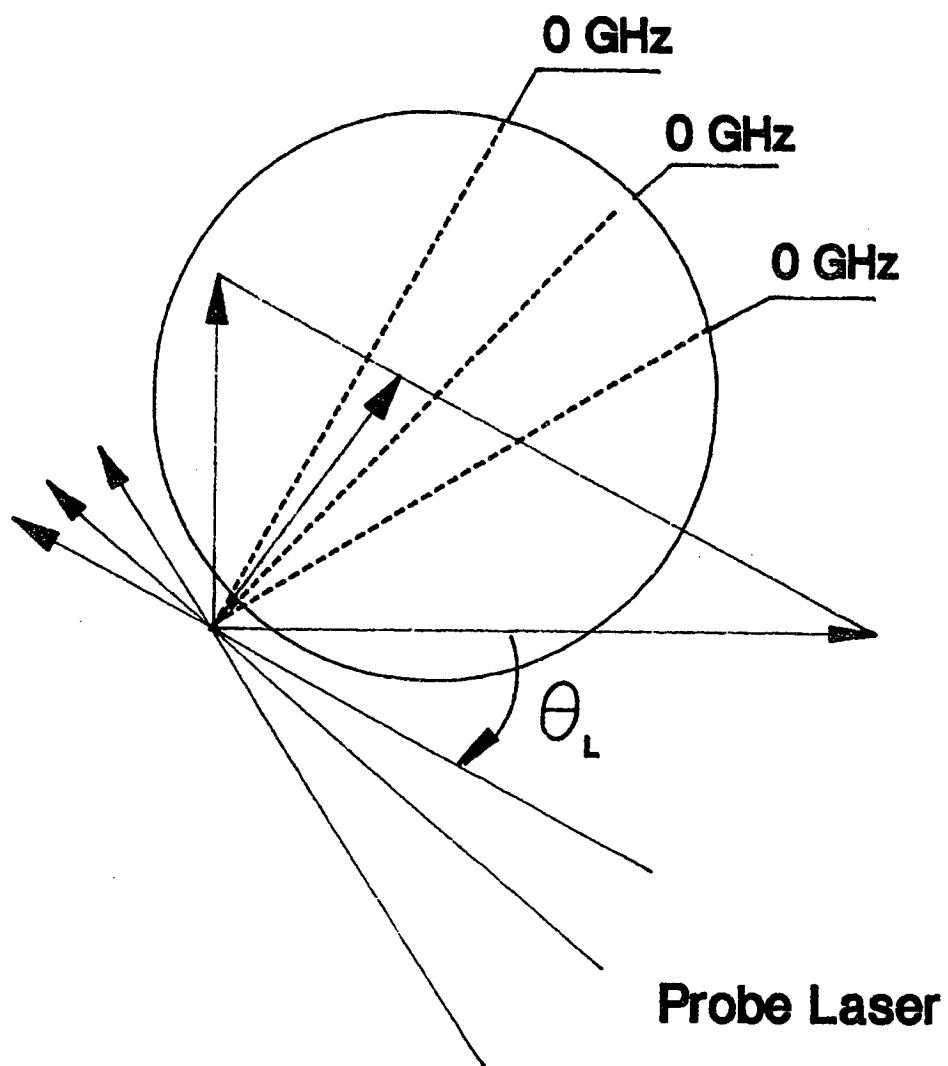


Fig. 3

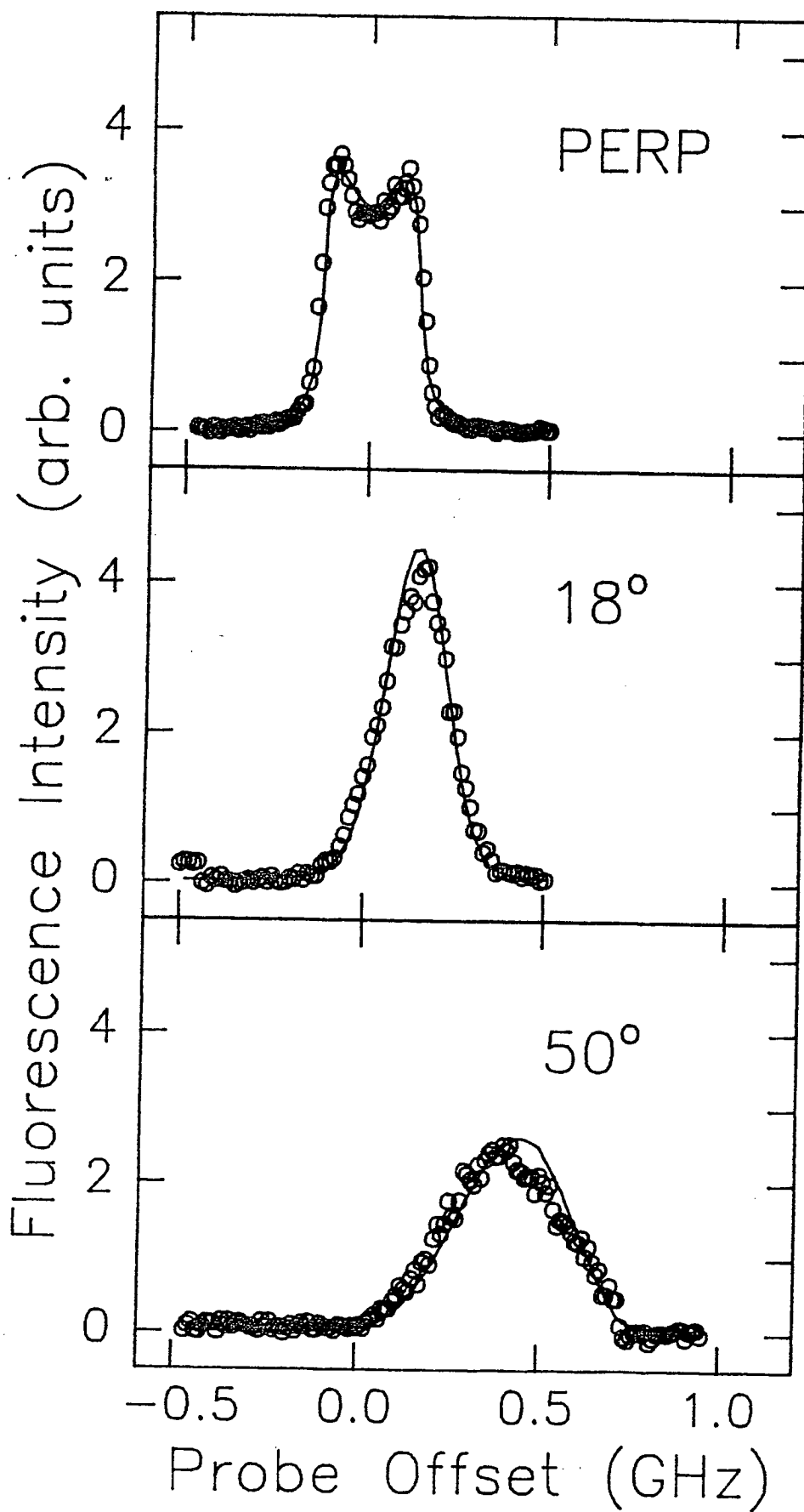


Fig. 4

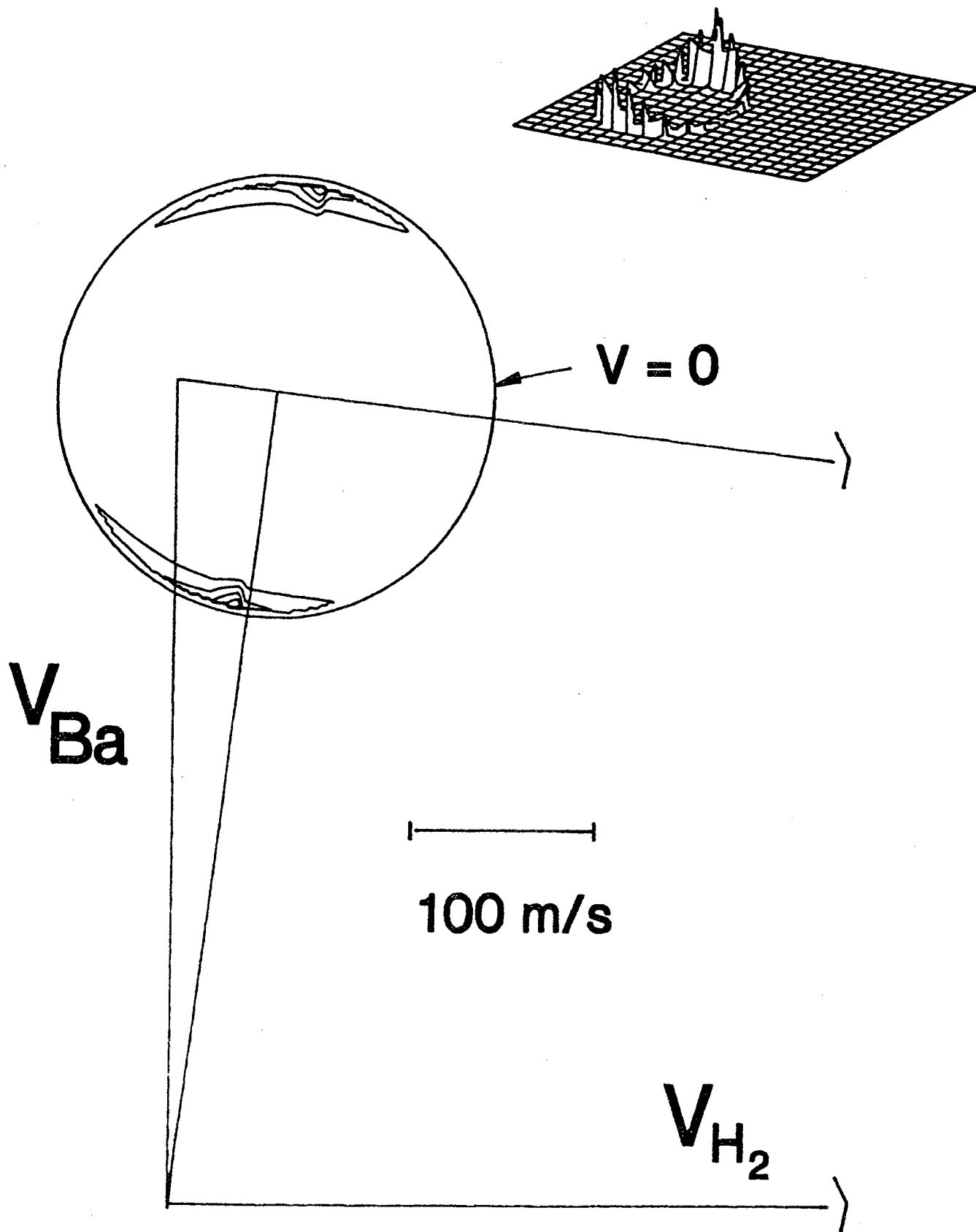


Fig. 5

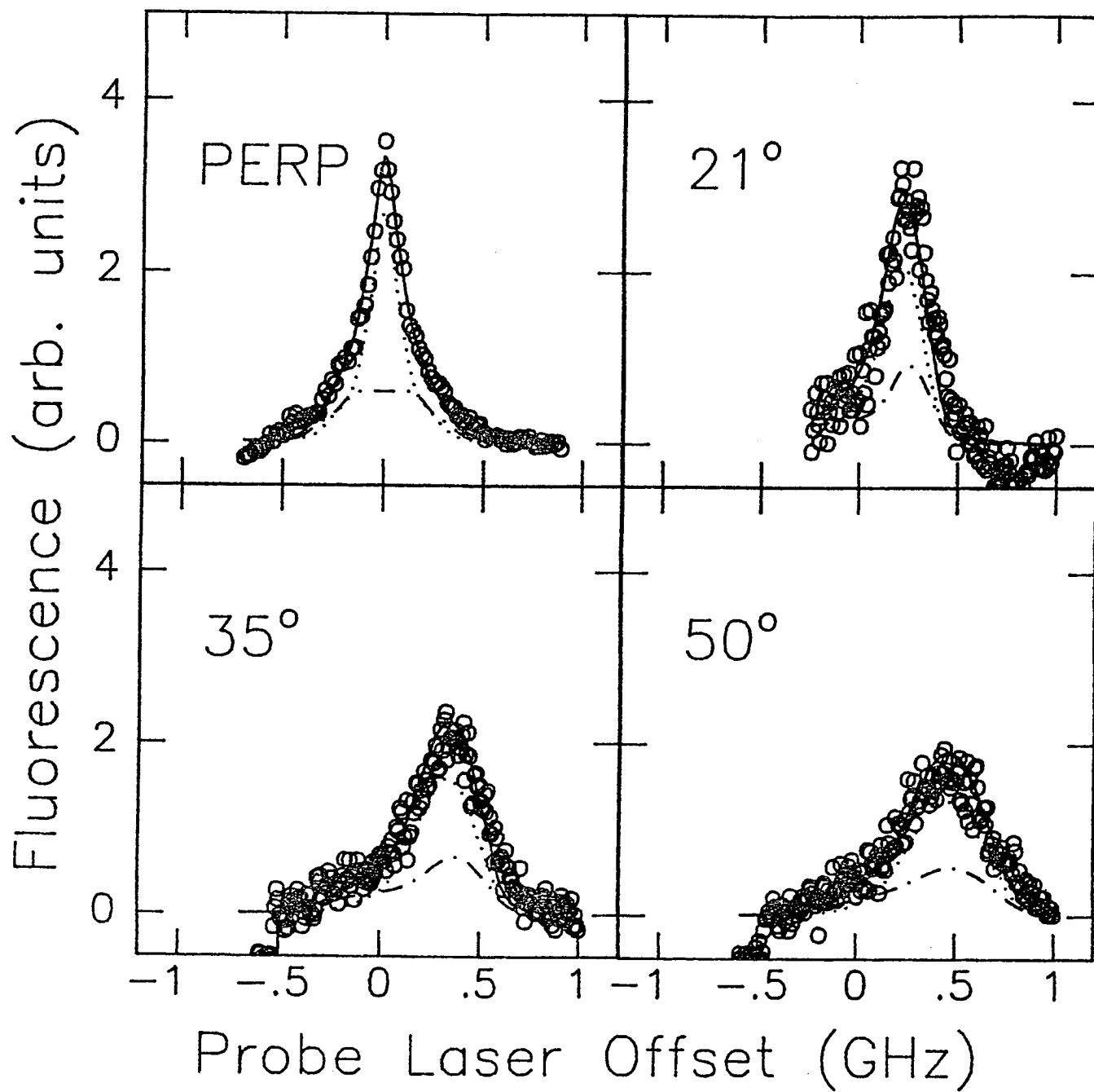


Fig. 6

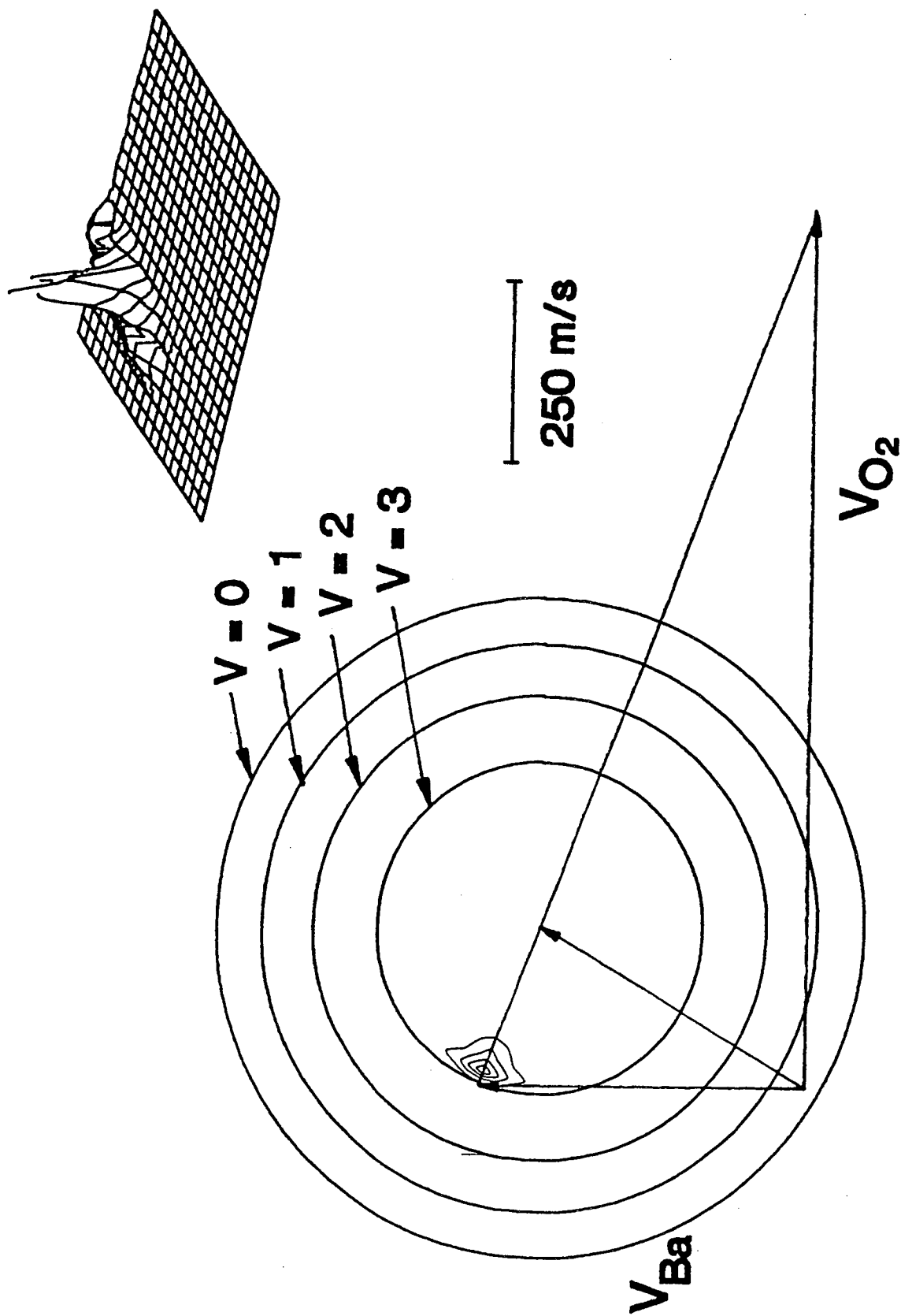


Fig. 7

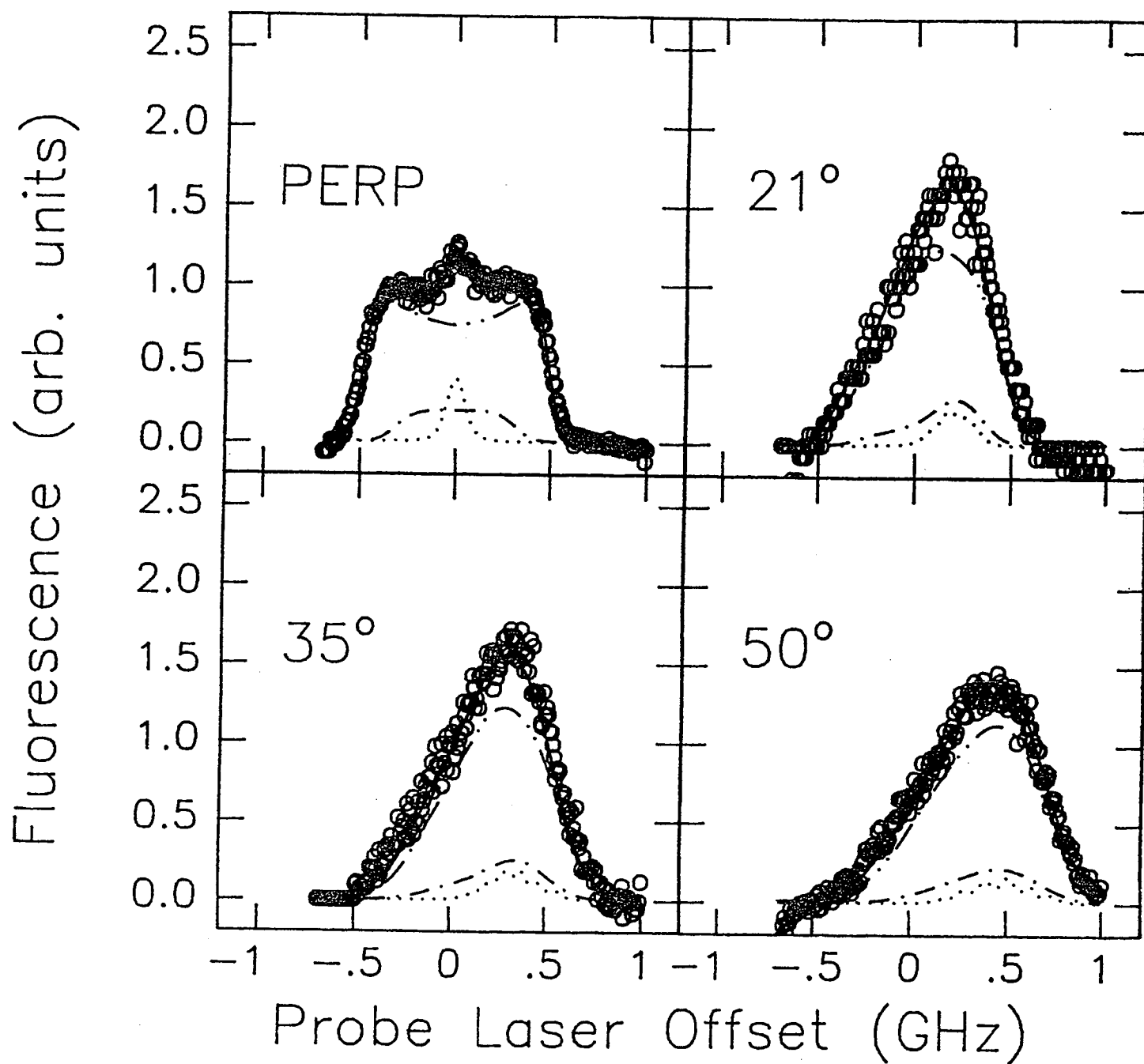


Fig. 8

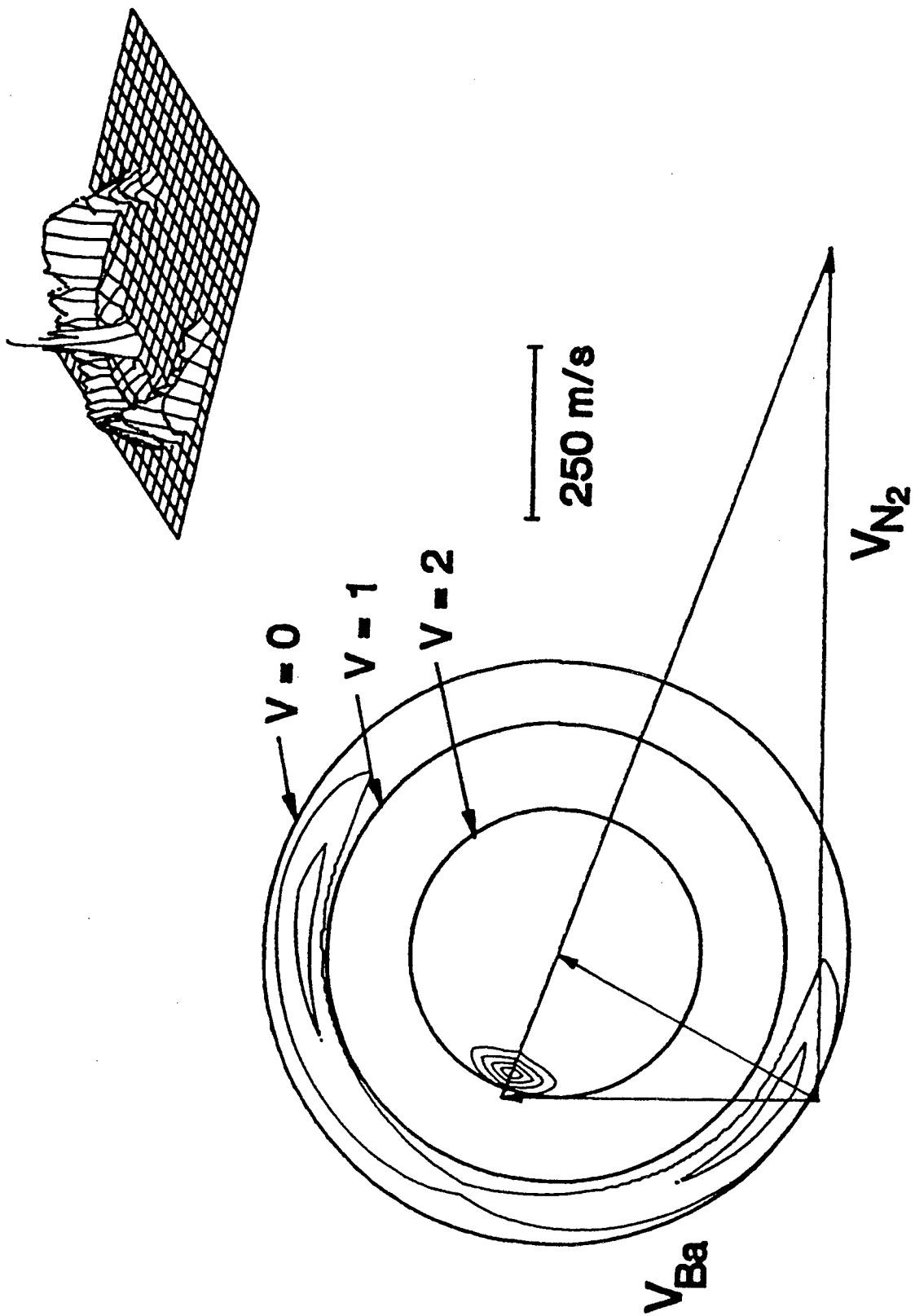


Fig. 9

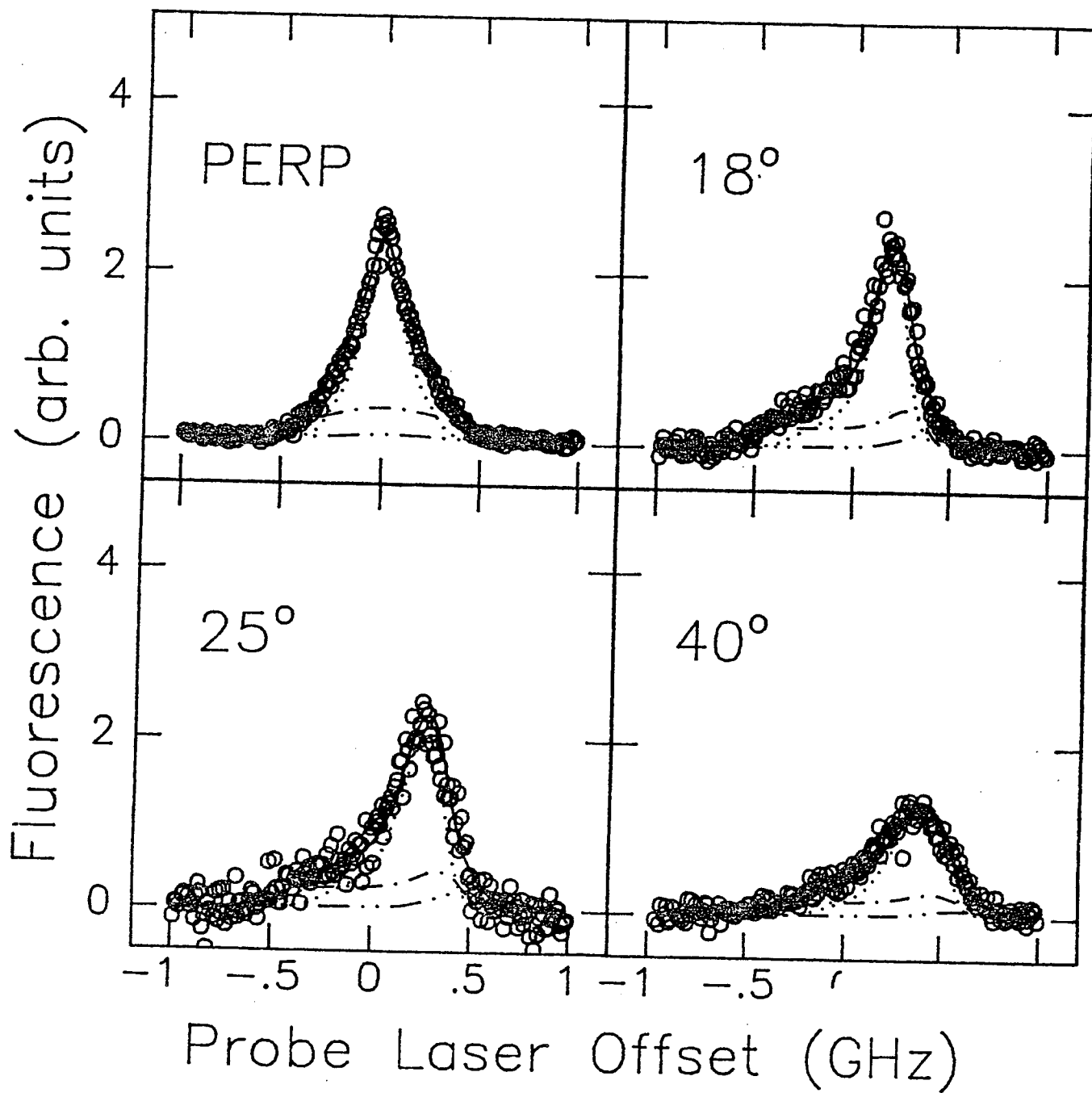


Fig. 10



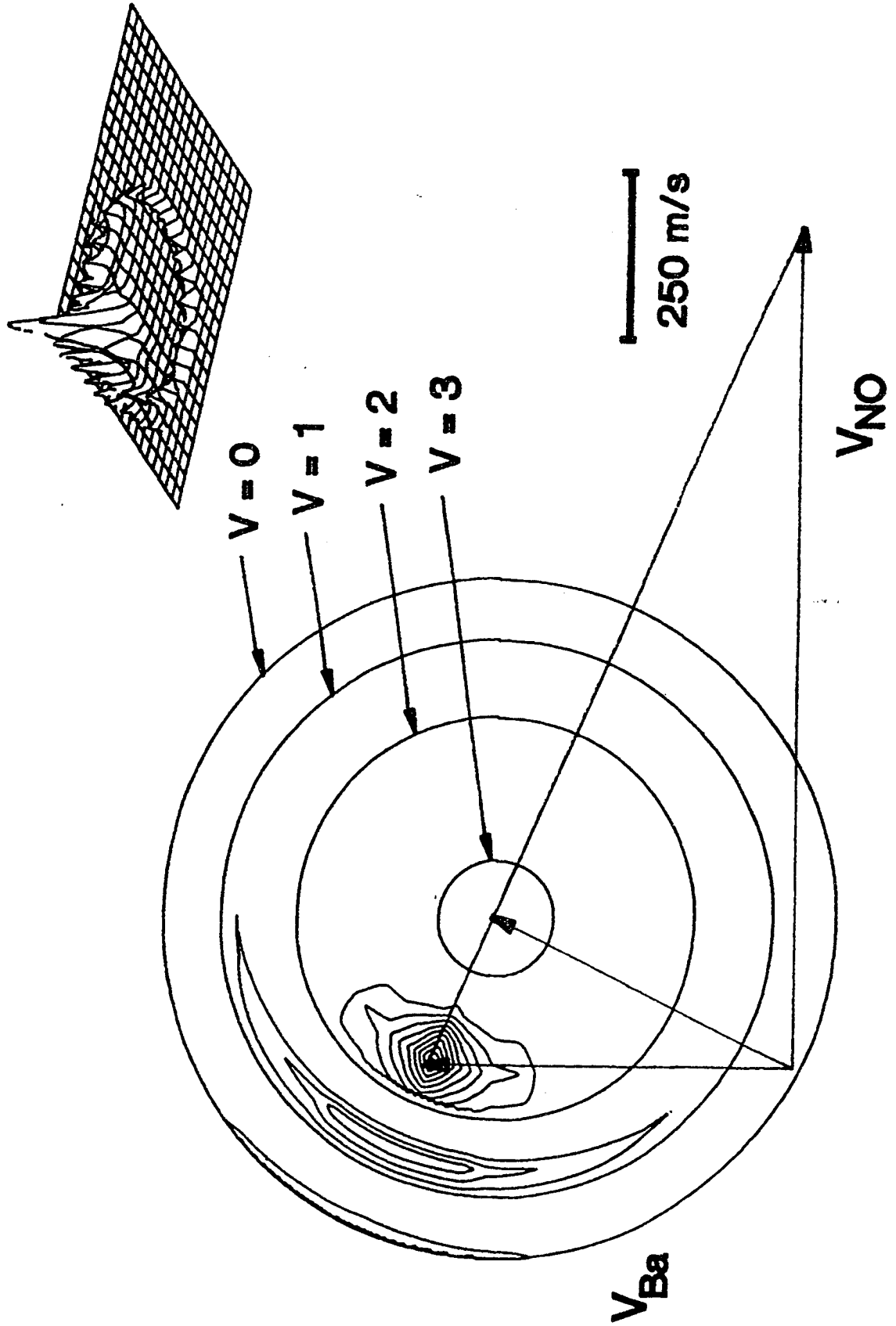


Fig. 11

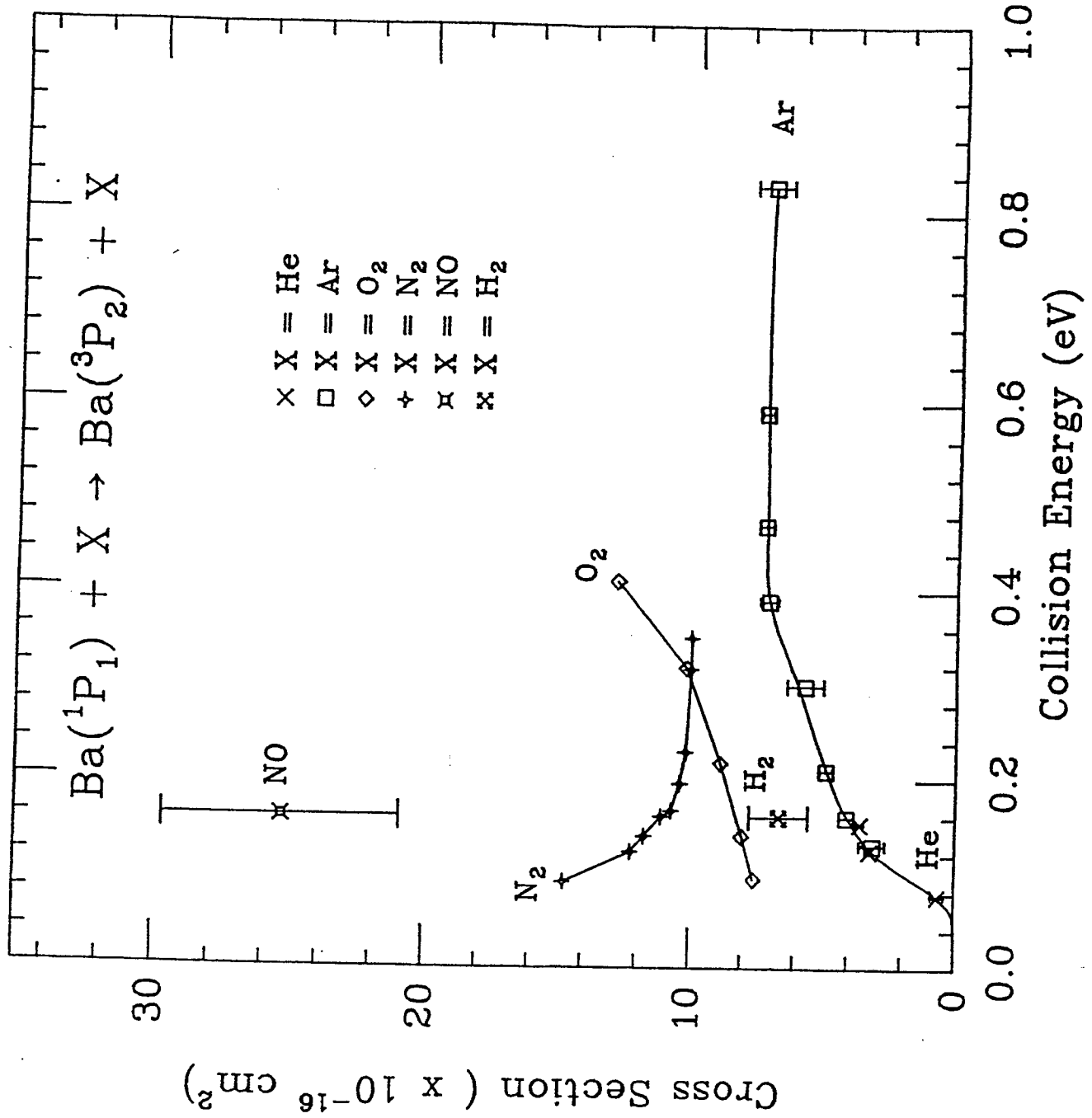


Fig. 12

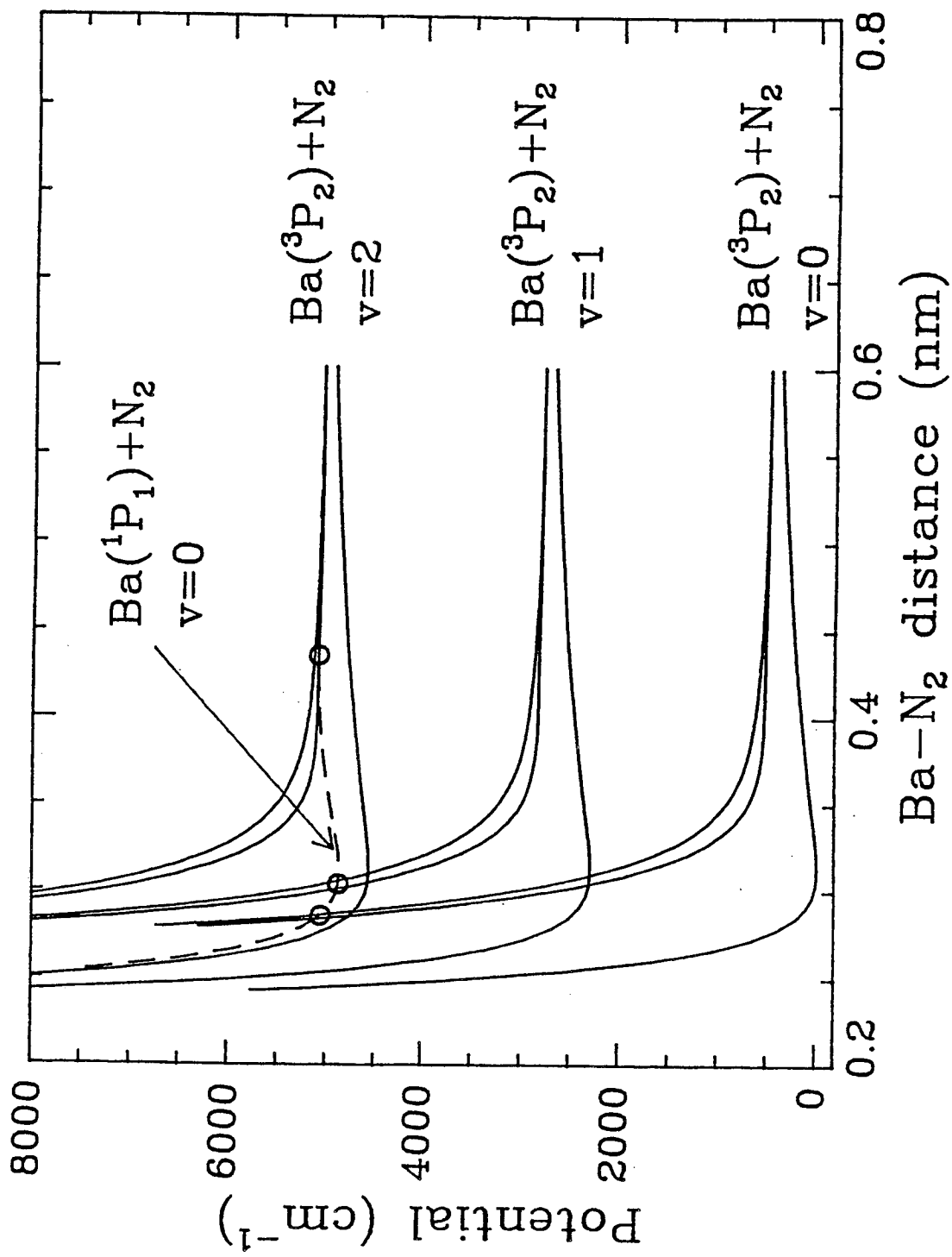


Fig. 13

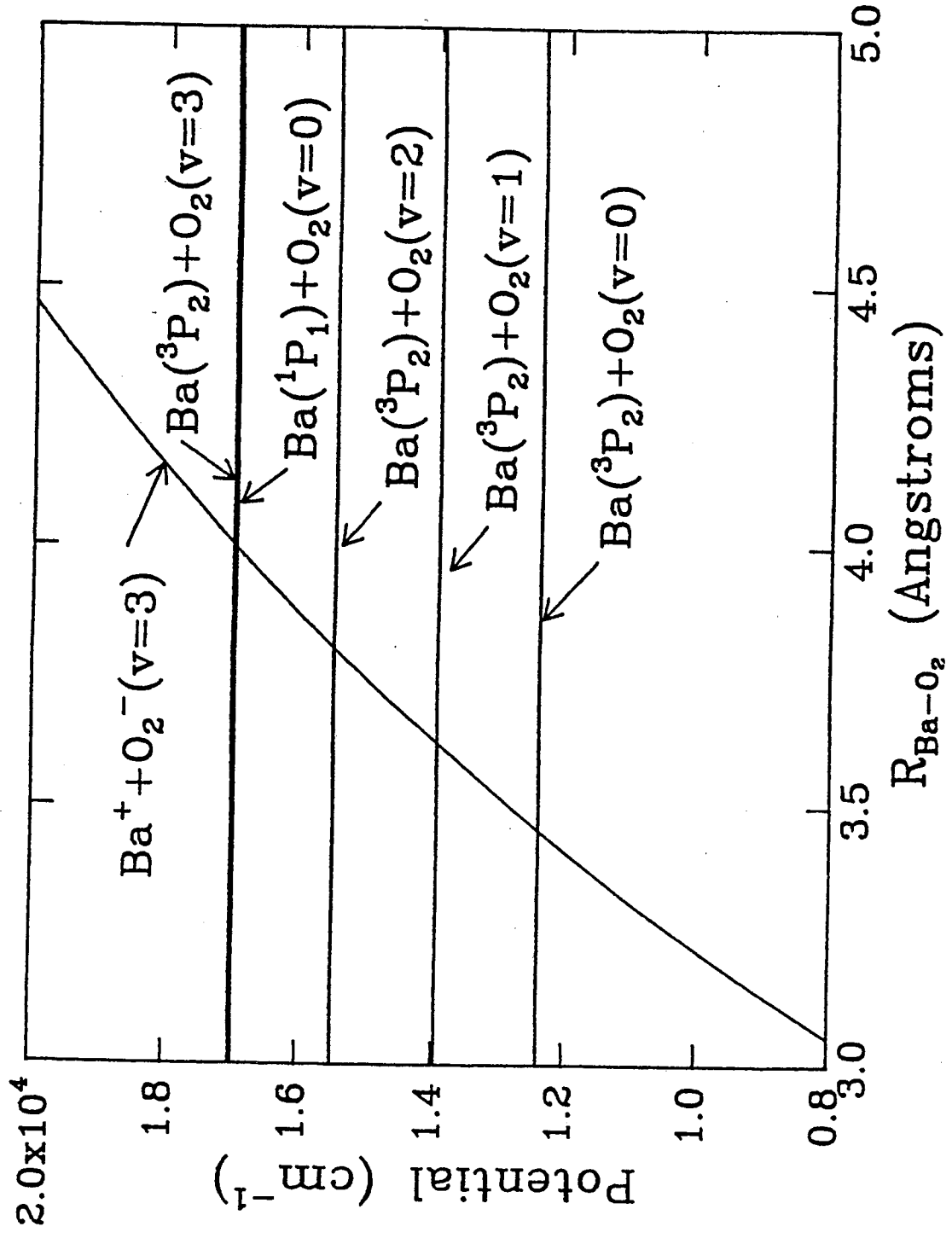


Fig. 14

LAWRENCE BERKELEY LABORATORY  
UNIVERSITY OF CALIFORNIA  
TECHNICAL INFORMATION DEPARTMENT  
BERKELEY, CALIFORNIA 94720